clear that the intrinsic resonance frequency f_2 is not changed by using any of the slot types. Fig. 4 shows the measured H-plane (x - z plane) radiation patterns with the dumb-bell slot at f_1 = 1.49GHz and f_2 = 1.94GHz, respectively. f_1 is the matching resonance frequency of the rectangular patch with the dumb-bell slot on the ground plane. f_2 is the intrinsic resonance frequency of the rectangular patch without the dumb-bell slot on the ground plane, which was almost the same as the calculated resonance frequency 1.9GHz. These frequencies are used for PDC and PHS cell phone systems in Japan. $\theta = 0°$ and $\theta = \pm 180°$ is the z-direction, which is perpendicular to the rectangular patches. From these results, an almost omnidirectional radiation pattern with 5dB gain variation was obtained at f_1, and a bidirectional radiation pattern was obtained at f_2. Therefore, the proposed microstrip antenna can realise an omnidirectional radiation pattern or a bidirectional radiation pattern simultaneously.

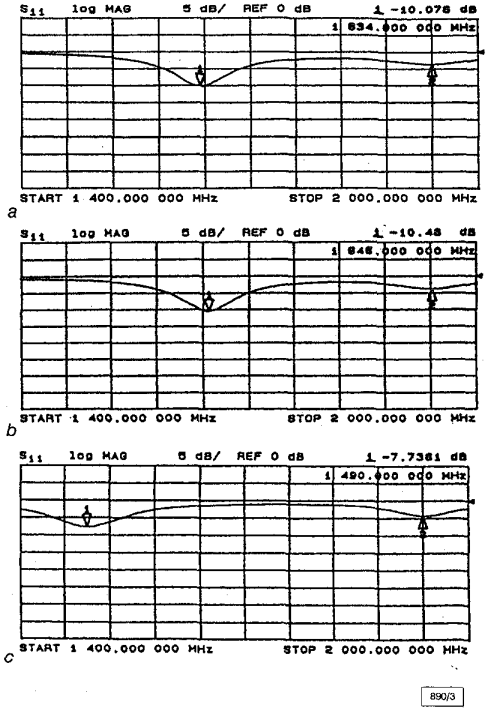

Fig. 3 *Measured input impedance of many slot types*

L = 150.0mm, t = 1.6mm, ε_r = 2.6, L_a = 47.3mm, L_s = 20.0mm, W_s = 1.0mm
a Rectangular slot
b Cross-slot
c Dumb-bell slot

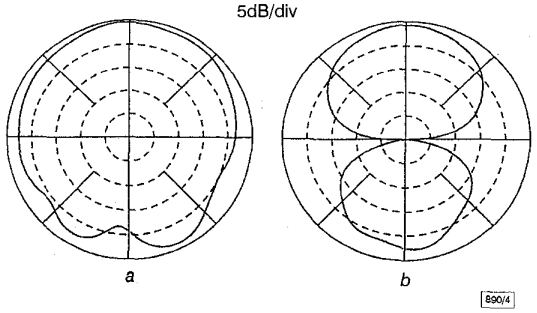

Fig. 4 *Measured radiation patterns by using dumb-bell slot*

L = 150.0mm, W = 35.0mm, t = 1.6mm, ε_r = 2.6, L_a = 47.3mm, W_a = 35.0mm, L_s = 20.0mm, W_s = 1.0mm
a f_1 = 1.49GHz
b f_2 = 1.94GHz

Conclusion: This Letter has described the experimental results for a proposed new microstrip antenna, which has a back-to-back configuration relative to a slot on a ground plane. An omnidirectional radiation pattern or a bidirectional radiation pattern are realised by using the proposed antenna configuration.

Electronics Letters Online No: 19980998 *4 June 1998*

H. Iwasaki (*Wireless Communications Technology Center, Toshiba Corporation, 3-1-1 Asahigaoka, Hino, Tokyo, 191-8555, Japan*)

References

1 KARIKOMI, M., MATSUOKA, T., and CHEN, L.W.: 'An omnidirectional broad band with microstrip antenna using a parasitic cylinder', *IEICE Trans. Commun.*, 1993, **E76-B**, (12)
2 CHO, K., and HORI, T.: 'Bidirectional rod antenna composed of narrow patches'. IEEE AP-S Symp., 1994, pp. 174–177
3 IWASAKI, H.: 'A microstrip array antenna with omnidirectional pattern fed by CPW'. IEEE AP-S Int. Symp., 1996, pp. 1912–1915
4 BAHL, I.J., and BHARTIA, P.: 'Microstrip antennas' (Artech House, Norwood, MA, 1980), pp. 86–90

Planar retrodirective array reflector using dual-slot antennas

Wen-Jen Tseng, Chun-Shu Hu and Shyh-Jong Chung

An X-band planar reflector with a broad responding beam was developed using the Van Atta retrodirective antenna array. The reflector contained four antenna sub-arrays, each with six dual-slot antennas appropriately fed and paired by microstrip lines on the backside of the substrate. Good agreement has been achieved between theoretical and measured results.

Introduction: Over the last two decades, the automotive collision avoidance system has become an important and interesting area for applications of microwave and millimetre-wave technologies. In the near future, it will serve as the basic vehicle equipment for intelligent transportation systems (ITS) [1]. Many investigations have been focused on the developments of vehicle radars [2, 3]. The radar emits a modulated continuous-wave (CW) or pulsed-wave to the environment and receives echoes from other vehicles or roadside obstacles. However, the microwave/millimetre-wave echo from a nearby vehicle relies on the scattering of the vehicle body, which is very narrow-beamed. Only near the normal direction to a body's surface can a high returning field be obtained. A consequent result associated with this phenomenon is searching blindness of the vehicle radar, which may cause a misjudgment and lead to a possible collision with nearby vehicles.

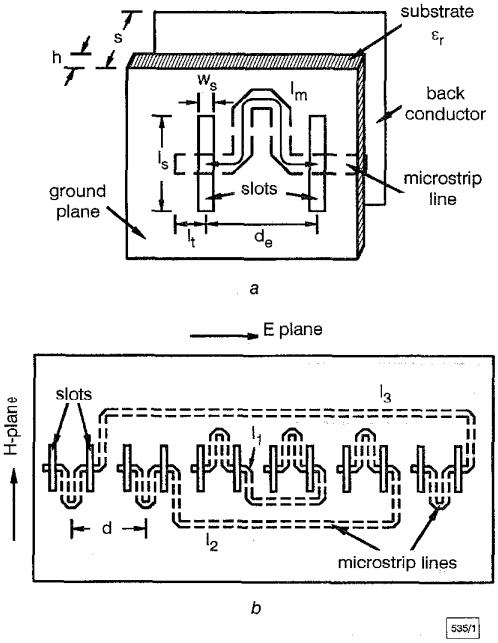

Fig. 1 *Geometry of dual-slot antenna and top view of six-element (1 × 6) Van Atta retrodirective sub-array*

a Geometry of dual-slot antenna
b Top view of sub-array

One possible solution to avoid the radar searching blindness is to equip planar retrodirective array reflectors on the body surfaces of a vehicle [4]. A retrodirective antenna array possesses the advantage that the reradiation field from all the elements of an array has a coherent phase in the arrival direction of the incident wave, thus yielding a broad back-scattering field pattern. In this Letter, we describe a passive planar Van Atta retrodirective array using dual-slot antennas (see Fig. 1). The Van Atta type array [5], where the antennas are located and paired symmetrically, is a commonly used retrodirective array. Since the microstrip lines linking the slot antenna are hidden behind the ground plane, the spurious radiation from these lines can be reduced to a minimum. Furthermore, use of an antenna with two slots can increase the antenna gain, thus raising the level of the reradiation field.

Retrodirective reflector configuration: Fig. 1*a* illustrates the geometry of a dual-slot antenna, which is formed by cascading two slots via a connecting microstrip line. Owing to the characteristic of the slot antenna that half of the power radiates backwards, a metal plate is placed behind the antenna to enhance the forward radiating power. The two slots are chosen to have the same dimensions and the length l_m of the connecting microstrip line is designed as one guided wavelength λ_m, so that the antenna possesses broadside and symmetric radiation. A Van Atta retrodirective antenna subarray containing six dual-slot antennas (1 × 6) is shown in Fig. 1*b*, where the antennas located symmetrically with respect to the array centre are paired by microstrip lines of lengths l_1, l_2 and l_3. To obtain a coherent array phase in the wave-arrival direction, the microstrip line lengths l_1, l_2 and l_3 should either be the same, or have differences which are multiples of λ_m [5].

The total back-scattering field from the array is mainly composed of two parts: the reradiation field from the antenna pairs (i.e. the field received by one antenna and reradiated by the other antenna in the same pair), and the scattering field from the finite substrate-loaded ground plane. Applying the method of moments together with a mixed potential integral equation (MPIE), the induced magnetic currents on the slots and the excited modal amplitude of the quasi-TEM mode in the microstrip line are obtained [6], from which the reradiation field is accessible. To simulate the scattering field of the ground plane, physical optics (PO) and the method of equivalent currents (MEC) are used [7].

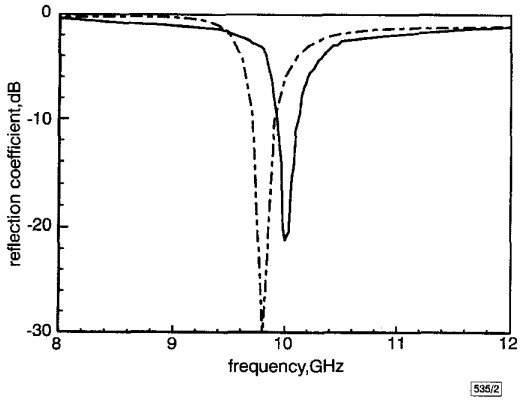

Fig. 2 *Measured and calculated frequency responses of dual-slot antenna*

ε_r = 2.2, l_s = 9mm, w_s = 1mm, l_t = 0.52mm, $l_m = \lambda_m$ = 21.76mm, d_e = 9mm, h = 0.508mm, s = 4.8mm
– – – calculated
——— measured

Results: A single dual-slot antenna was designed and measured. Fig. 2 shows the calculated and measured frequency responses of the return loss. (The structure parameters are listed in the captions.) The measured return loss is 21.2dB at the centre frequency of 10GHz which is 2% off the calculated one (9.8GHz).

The retrodirective array reflector was constructed by combining four identical sub-arrays (each as shown in Fig. 1*b* in the H-plane with a distance of 25.5mm (= 0.85 free-space wavelength (λ_0)). The spacing between antennas in a sub-array was 18mm (= 0.6 λ_0). This 4 × 6 array reflector measured a size of 127 × 120mm^2. The 50Ω microstrip lines connecting the antenna pairs were designed to be with lengths of l_1 = 37.493mm, $l_2 = l_1 + 2\,\lambda_m$ = 81.013mm, and $l_3 = l_1 + 3\,\lambda_m$ = 102.773mm.

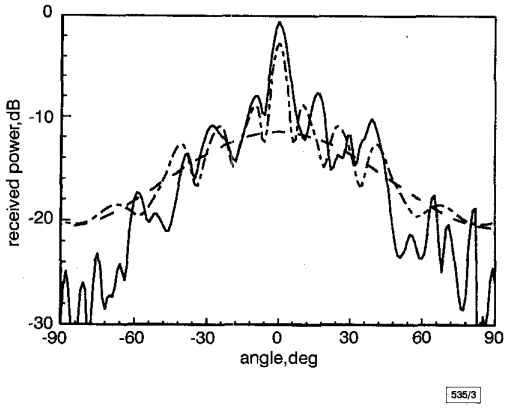

Fig. 3 *Comparison between measured and calculated field patterns of 4 × 6 retrodirective array reflector*

f = 10GHz, d = 18mm, l_1 = 37.493mm, $l_2 = l_1 + 2\,\lambda_m$ = 81.013mm, $l_3 = l_1 + 3\,\lambda_m$ = 102.773mm, λ_m = 21.76mm
– – – – calculated reradiation
– · – · calculated total
——— measured total

The measured and calculated E-plane back-scattering patterns of the 4 × 6 retrodirective array reflector at 10GHz are shown in Fig. 3. The patterns are normalised to the maximum value (at 0°) of the back-scattering field from a metal plate of the same size as the reflector. For reference, the calculated reradiation-field pattern is also shown. Basically, this pattern is the square of the radiation pattern of a dual-slot antenna [4]. The main lobe (at 0°) of the total-field pattern is due to the high scattering field from the ground plane near the normal direction. Outside the main lobe, the variations in the total-field pattern eventually follow those of the reradiation-field pattern. The small ripples come from the interference of the ground-plane scattering field. These results indicate that the reradiation field dominates the total back-scattering field outside the main lobe region, thus enhancing the beamwidth of detection. As can be seen, the experimental measurements are very close to the predicted values.

Conclusion: In this Letter, a Van Atta retrodirective array reflector, using dual-slot antennas for operation at 10GHz, has been designed and demonstrated experimentally. The method of moments together with an MPIE and the PO method coupled with MEC were used to analyse the structure. The theoretical results agreed quite well with the experimental measurements.

Acknowledgment: This work was supported by the National Science Council of the Republic of China under grant NSC 87-2213-E-009-115.

18 May 1998
Electronics Letters Online No: 19980983

Wen-Jen Tseng, Chun-Shu Hu and Shyh-Jong Chung (*Department of Communication Engineering, National Chiao Tung University, 1001 Ta Hsueh Road, Hsinchu 30039, Taiwan, Republic of China*)

E-mail: sjchung@cm.nctu.edu.tw

References

1 FRENCH, R.L., and LAY, M.G.: 'The archaeology of intelligent transportation systems', *IEEE Veh. Technol. Soc. News*, 1997, pp. 33–36

2 CHANG, K.W., WANG, H., SHREVE, G., HARRISON, J.G., CORE, M., PAXTON, A., YU, M., CHEN, C.H., and DOW, G.S.: 'Forward-looking automotive radar using a W-band single-chip transceiver', *IEEE Trans. Microw. Theory Tech.*, 1995, **43**, pp. 1659–1668

3 STILLER, A., BIEBL, E.M., LUY, J.-F., STROHM, K.M., and BUECHLER, J.: 'A monolithic integrated millimeter wave transmitter for automotive applications', *IEEE Trans. Microw. Theory Tech.*, 1995, **43**, pp. 1654–1658

4 CHUNG, S.-J., and CHANG, K.: 'A retrodirective microstrip antenna array',1997 Progress in Electromagnetics Research Symp. (PIERS), 1997, (Hong Kong),pp. 131
5 VAN ATTA, L.C.: 'Electromagnetic reflector'. U.S. Patent 2,908,002, Serial no. 514,040, October 1959
6 TSENG, W.-J., and CHUNG, S.-J.: 'Analysis and application of a two-port aperture-coupled microstrip antenna', *IEEE Trans. Microw. Theory Tech.*, 1998, pp. 530–555
7 STUZMAN, W.L., and THIELE, G.A.: 'Antenna theory and design' (John Wiley & Sons, New York, 1981)

Current-mode analogue circuit representation of Hodgkin and Huxley neuron equations

C. Toumazou, J. Georgiou and E.M. Drakakis

A nonlinear current-mode circuit representation, suitable for a laboratorial realisation, of the Hodgkin and Huxley (HH) nerve axon membrane equations is presented. The representation exploits the inherent properties of the recently proposed 'Bernoulli cell' to calculate the intermediate state variables used in the HH neuron equations.

Introduction: Modelling the flow of electric current through the surface membrane of neurons has proved to be a classic problem. In Hodgkin and Huxley's electrical circuit model [1], 'time-varying linear conductances' are used to model the variable permeability of the nerve cell membrane to the various ions. Chua [2] first pointed out that the sodium and potassium conductances, g_{Na} and g_K, respectively, could be classified as 'non-linear time-invariant memristive one-ports'. Parodi and Storace [3] exploited Chua's formalism and indicated that the synthesis of the memristors could be achieved by using multi-port nonlinear time invariant resistors in conjunction with linear capacitors. The dimensionless state variables n, m and h in their HH circuit model were obtained by considering ratios of appropriately scaled voltages.

In this Letter, a different strategy is proposed; in contrast to a voltage-mode circuit model, a transistor level current-mode approach is adopted. Apart from being an alternative circuit representation of the HH dynamics, this approach offers a more realistic circuit implementation for the memristive blocks. More specifically, in this Letter the H-H equations are briefly presented and are then rearranged to fit the recently proposed 'Bernoulli cell' dynamics [4]. Simulations, confirming the resulting circuit representation, are also shown.

Circuit derivation: Hodgkin and Huxley consider a finite area portion of nerve axon membrane. Current can be carried either by charging the membrane capacity or by movement of ions (ionic current) through the time-variant conductances. The ionic current is divided into components carried by sodium and potassium ions (I_{Na} and I_K, respectively) and also a small leakage current (I_L) made up of chloride and other ions.

$$I = C_M \frac{dV}{dt} + I_{Na} + I_K + I_L \qquad (1)$$

where V is the displacement of the membrane potential from its resting value (depolarisation negative). Fig. 1 illustrates the corresponding electrical circuit proposed originally by HH.

The leakage current I_L is given by

$$I_L = (V - V_L)\bar{g}_L \qquad (2)$$

where V_L and $\bar{g}_L$ are empirically determined. The potassium conductance g_K is given by

$$g_K = \bar{g}_K n^4 \qquad \frac{dn}{dt} = \alpha_n(1-n) - \beta_n n \qquad (3)$$

where $\bar{g}_K$ is a fixed-value conductance, α_n and β_n are voltage dependent rate constants of dimension $[s]^{-1}$ and n is a dimensionless state-variable representing 'potassium activation'.

In [4] it was shown that the dynamic behaviour of the circuit illustrated in Fig. 2*a*, comprising an *npn* base junction transistor (BJT) and an emitter connected (linear) grounded capacitor, can be described by means of a Bernoulli differential equation. This circuit was termed a 'Bernoulli cell' (BC) and when logarithmically driven, as in Fig. 2*b*, it can be shown that it realises the following differential equation:

$$CV_T\dot{w}_1 + I_{u1}w_1 = I_{IN1} \qquad (4)$$

with $w_1 = I_{IN1}/I_C$ and C being the value of the capacitor. A simple manipulation of eqn. 3 gives

$$CV_T\frac{dn}{dt} + CV_T(\beta_n + \alpha_n)n = CV_T\alpha_n \qquad (g_K = \bar{g}_K n^4) \qquad (5)$$

A direct comparison reveals that eqn. 5 has the form of eqn. 4 when n is analogous to the dimensionless ratio of currents w_1, and when $CV_T\alpha_n$, and $CVT(\beta_n + \alpha_n)$ correspond to I_{IN1} and I_{u1}, respectively. Hence, the currents I_{IN1} and I_{u1} can be viewed as being driven by time-invariant, voltage dependant, nonlinear current sources. The output current $I_{out1} = I_0 w_1$ (see Fig. 2*c*) 'senses' the w_1 variable via a translinear loop [5]. The potassium ionic current can thus be generated by means of a time invariant nonlinear current source, which is controlled by a ratio of currents, w_1, and the membrane potential displacement V.

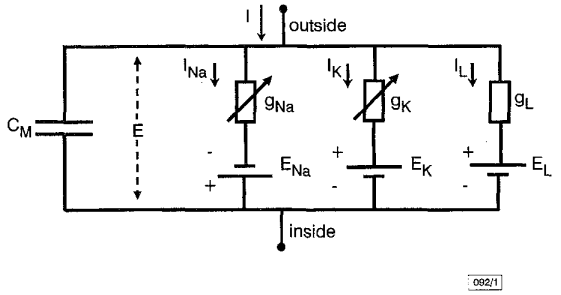

Fig. 1 *H-H electrical circuit representing nerve axon membrane*

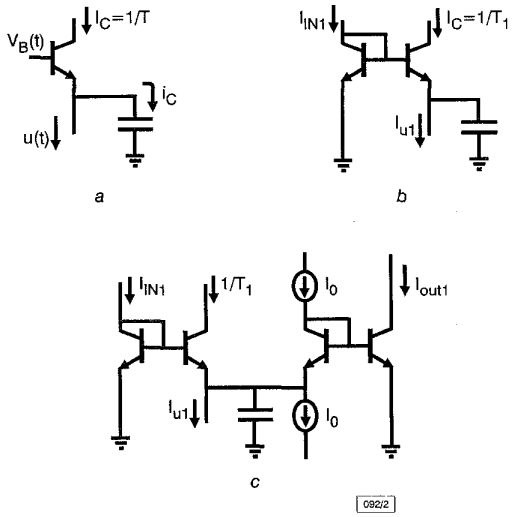

Fig. 2 *Bernoulli cell and logarithmically-driven Bernoulli cell with and without state 'sensing'*

a Bernoulli cell
b Logarithmically-driven Bernoulli cell
c Logarithmically-driven Bernoulli cell with state 'sensing'

Similar thoughts also apply to the sodium conductance ($g_{Na} = \bar{g}_a m^3 h$). The dynamic behaviour of its state variables can be described by the following pair of differential equations:

$$CV_T\frac{dm}{dt} + CV_T(\beta_m + \alpha_m)m = CV_T\alpha_m \qquad (6)$$

$$CV_T\frac{dh}{dt} + CV_T(\beta_h + \alpha_h)h = CV_T\alpha_h \qquad (7)$$

Eqns. 6 and 7 can be realised using two logarithmically-driven BCs of the form shown in Fig. 2*b* and *c* and incorporating appropriate nonlinear current sources as was performed for the potassium conductance.